Heterogeneity of microstructure, texture and mechanical properties along the building direction of Ti-6Al-4V alloy developed by SLM

C Widomski, D Solas, T Baudin, F Brisset, S Lebel, A L Helbert

Heterogeneity of microstructure, texture and mechanical properties along the building direction of Ti-6Al-4V alloy developed by SLM

C. Widomski[1], D. Solas[1], T. Baudin[1], F. Brisset[1], S. Lebel[2], A.L. Helbert[1,*]

[1]*Université Paris-Saclay, CNRS, Institut de chimie moléculaire et des matériaux d'Orsay, 91405 Orsay, France.*
[2]*AddUp, 5 Rue Bleue, 63118, Cébazat, France.*

Abstract

Selective Laser Melting (SLM) is of great interest to the aerospace industry due to its ability for producing components with complex geometries. The laser melting process induces a high cooling rate (10^5-10^7 K/s) and a germination by epitaxy which leads to a columnar microstructure. In the case of Ti-6Al-4V the rate of cooling from the β domain generates a martensitic α' structure made up of fine needles. The present work describes the microstructural, textural and mechanical heterogeneities along the building direction of Ti-6Al-4V samples produced by SLM with two strategies that have different melt pool size. Characterizations show that both strategies lead to a martensitic microstructure but only the SLM with the greater melting area allows to get homogeneous hardness, texture and β grain size (reconstructed by ARPGE) along building direction.

1. Introduction

The Selective Laser Melting (SLM) powder bed process is probably the most attractive technique for building parts with a high degree of complexity as indicated in the work by Kruth et al. [1]. The manufacturing of a product is formed by selectively melting successive layers of powder with the interaction of a laser beam. The Ti-6Al-4V titanium alloy is one of the most common alloys elaborated by the SLM process because it is widely used in aerospace and biomedical applications. The mechanical properties of Ti-6Al-4V alloy obtained by this process have been intensively studied in the literature [2] [3]. One of the challenges facing additive manufacturing process is the ability to achieve identical microstructure and mechanical properties throughout the elaborate piece. The high cooling rate of the SLM process generates Ti-6Al-4V parts with predominant martensitic α′ microstructure where prior β grains grow epitaxially throughout the deposition layers. The β grain solidification is influenced by the laser scan strategy and the β phase has a strong 〈100〉 texture along its grain growth direction parallel to the Z-axis [4] [5]. This rapid solidification behavior is due to large thermal gradients along the building direction that generates the parts with high strength and low ductility, residual stresses and solidification texture that induce anisotropy in the final product [6] [7]. Some studies reported that despite the fact that each layer is thermally affected by the deposition of a new one, the morphology and size of the α' grains change along the building direction [8] [9]. The aim of this work is to compare the microstructures obtained with two different strategies and to check their homogeneity along the building direction. A new strategy called Laser Boost (LB), is compared to the Classical Linear (CL) one. The LB process allows a wider melting area in order to improve melt flow rate and mechanical properties. Scanning Electron Microscope (SEM) and Electron BackScatter Diffraction (EBSD) were used to characterize the microstructure and the texture. EBSD data were used to reconstruct the prior β grains, in order to study the grain solidification microstructure. The quantification of β-phase was performed using X-ray diffraction to follow the microstructure evolution along building direction and mechanical properties were characterized by micro hardness.

2. Experimental conditions

2.1 Material and process

The powder of Ti-6Al-4V alloy (titanium base, 6% aluminum and 4% of vanadium wt.%) was manufactured by gas atomization method and the spherical particle size ranged from 5µm to 25µm. In this study, all samples were produced by AddUp company using a FormUp 350 SLM machine. Because of the high chemical reactivity of titanium alloys with oxygen, the build chamber was filled with argon. With the layer-by-layer process deposits, metal epitaxially regrows from the previously fused layer. Moreover, the high temperature gradient with a cooling rate of 10^5-10^7 K/s [10] [11] generates a columnar structure of β grains with a solidification direction parallel to the $<001>_\beta$ crystallographic direction. The Ti-6Al-4V fabricated by SLM process generates α′ martensitic laths that originate from the parent β grains precipitate according to the Burgers orientation

relationship. In this study, CL and LB strategies were compared. The LB strategy uses a larger melting area with a higher power and a lower scan speed in comparison to the CL strategy. Cylindrical bar-shaped samples of each strategy were built vertically, parallel to Z-axis (Fig. 1(a)), with a laser scanning path using unidirectional scanning with a 90° rotation between each layer. After fabrication, the samples underwent a stress-relieve treatment at 540°C during 2h under argon followed by furnace cooling. To study the heterogeneity of mechanical properties in the parts along the building direction, one pellet is taken at the TOP and one at the BOTTOM of each bar elaborated with CL and LB strategies. The characterization is conducted on the pellet surface perpendicular to Z-axis (Fig. 1(b)).

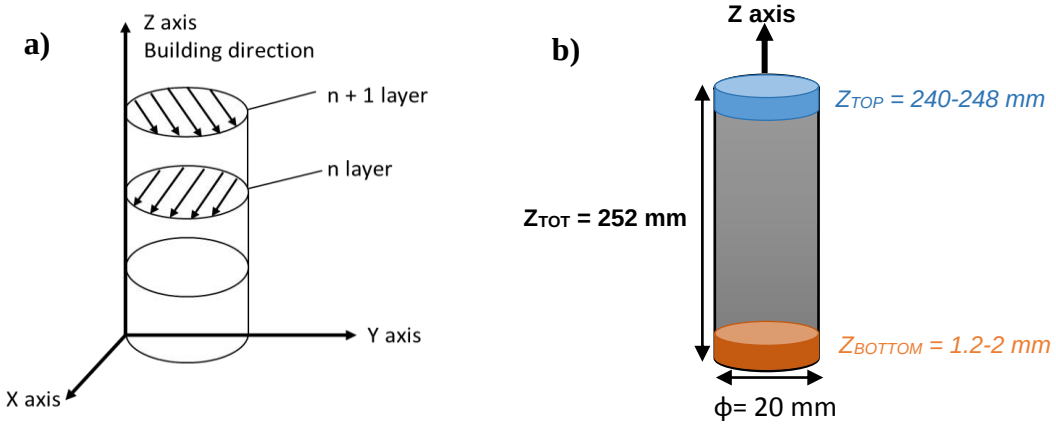

Fig. 1: (a) Laser scanning path (b) Position of the TOP and BOTTOM pellet in the bar shaped sample

The Volume Energy Density (VED) (J/mm^3) was calculated for both strategies as follows (Eq.1):

$$VED = \frac{P}{V_s \times H \times L} \quad (1)$$

With P = laser power (W), V_s = scan speed (mm/s), H = layer thickness (mm), L = spacing between laser hatching vectors (mm). The CL is performed with a VED of 47.2 J/mm^3 and the LB with a VED of 53.6 J/mm^3. The main advantage of the LB strategy is that it allows to melt a larger quantity of powder. The melting rate of the SLM process ($H \times L \times V_s$) is about 13 cm^3/h for the CL strategy and 49 cm^3/h for the LB strategy.

2.2 Microstructure and mechanical characterization

Examination of the microstructure in the (XY) plane occurred after grinding with SiC paper up to a fine 2400 grid size and then an electro-chemical polishing is carried out with the Struers A3 solution. Microstructure and crystallographic orientations were examined by EBSD. Due to the stress-relieved and the Z-position of the pellets, a fraction of martensitic microstructure may have returned to equilibrium phases (α+β). To quantify this phase transformation, the proportion of β-phase was measured from XRD diffraction diagrams using $(110)_\beta$ and $(0002)_\alpha$ peak intensities [12]. According to the Burgers orientation relationship, these two planes are parallel. The fabrication by SLM induces a grain orientation such that the <001> direction of the β-phase is parallel to Z-axis. As a consequence, the $\{110\}_\beta$ planes are inclined at 45° relative to Z-direction. A texture goniometer is used because it allows to tilt the sample with an χ-angle between 40 and 50° in order to place itself in the Bragg conditions to measure the $(110)_\beta$ and $(0002)_\alpha$ peak intensities .This phase identification was performed on (XY) plane, using XRD with an Inel CPS 120 curved detector. The XRD patterns were obtained with in a χ range from 40° to 50° with an increment of 2.5° and a φ between 0°-355° with an increment of 5°. The mechanical properties were evaluated by Vickers micro hardness. The average and the standard deviation correspond to 7 measures with a load of 0.3kg during 15s realized on the (XY) plane of each pellet.

3. Results

3.1 Martensitic microstructure along the building direction

The Fig. 2 shows EBSD Z-IPF of the (XY) plane obtained with both strategies. The microstructure is only composed of martensitic α' needles. The applied strategy does not change the α' microstructure of the Ti-6Al-4V alloy and there is no difference in needle size. With the CL strategy, α' needles have 2.5µm of width and 3 µm of width with LB strategy. According to the Burgers relation for the Ti-6Al-4V alloy, one β orientation

gives twelve α' orientations that's why the α' overall texture is random [13]. Nevertheless, the microstructure exhibits some domains which correspond to the prior β gain structure and they are larger for the LB process (Fig. 2(d)) compared to those obtained with the CL strategy (Fig.2 (b)).

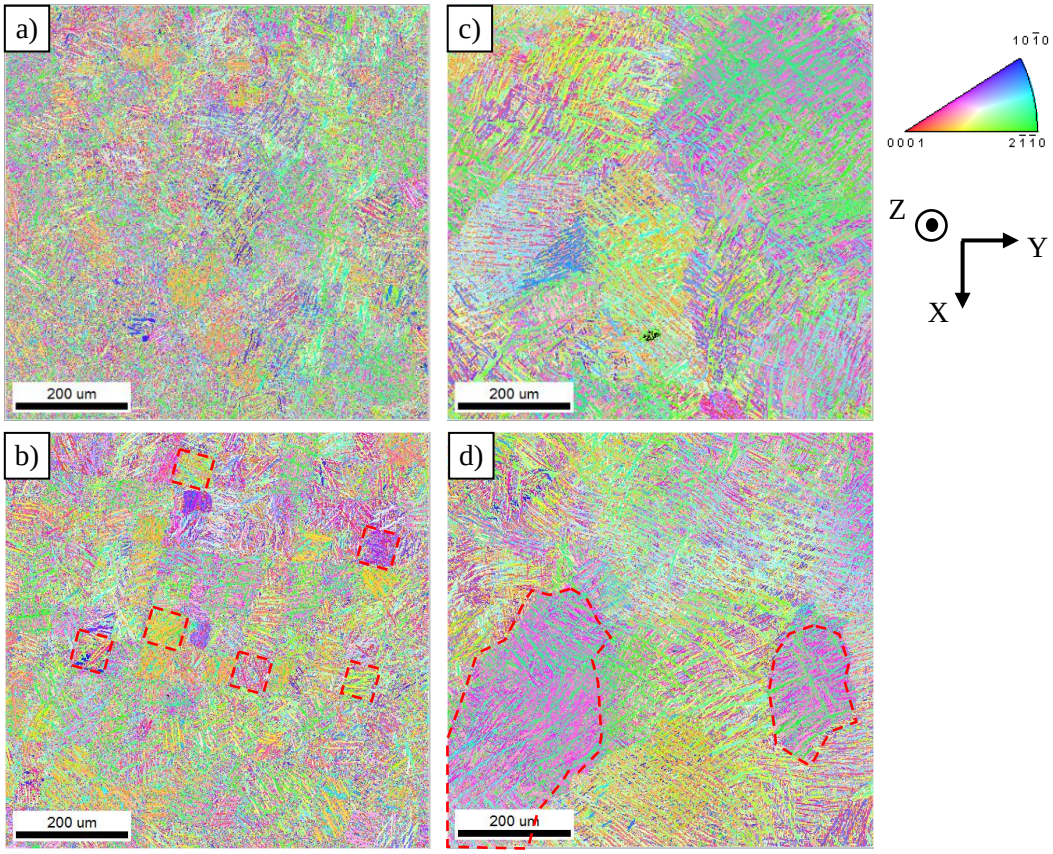

Fig. 2 : EBSD [001] Inverse Pole Figure (IPF) orientation map of α′ of Ti-6Al-4V SLM specimen obtained after stress relief at 560°C/2h. The IPF map showing the α′ microstructure and texture on the (a) TOP and on the (b) BOTTOM of a bar elaborated with CL strategy and on the (c) TOP and on the (d) BOTTOM elaborated with LB strategy.

3.2 β-phase morphology along building direction

Because the β phase is difficult to observe directly by EBSD, the corresponding maps were reconstructed from Fig. 2 (IPF α' maps) using the ARPGE software [14]. The reconstruction of the β grains is based on the Burgers crystallographic relationship that governs the α → β phase transformation and especially the directions relations $(0001)_\alpha$ // $(110)_\beta$ and $<111>_\beta$ // $< 11\bar{2}0 >_\alpha$. The Fig. 3 shows β-phase microstructures after reconstruction. The black areas are not porosity but areas that have not been reconstructed because there are not enough orientation variants. On the β-phase map corresponding to the CL laser strategy, small square areas are present due to the laser scanning direction that is rotated by 90° between each layer (Fig. 1). It generated periodic patterns in each layer that lead to a grid microstructure of β-phase with different crystallographic orientations. There is also a difference in grain size along the building direction. The β grains have a size in the order of 60 µm (± 9µm) at the BOTTOM and around 105 µm (± 9µm) at the TOP. This grain size increase from BOTTOM to TOP can be explained by grain growth selection and the temperature rise induced by thermal cycling with the CL strategy. The LB strategy induces larger melting area and therefore larger β grains are observed. The average size of β grains is 110µm (± 43 µm) at the BOTTOM and 102 µm (± 80 µm) at the TOP because of the homogeneous thermal cycling due to the LB strategy. Moreover, grain shape is irregular on contrary to the CL strategy.

In Fig. 3, the β-reconstructed orientation map and the IPF of the LB strategy highlight a preferential growth direction $<001>_\beta$ // Z. The texture of the LB sample is similar along the building direction. For the CL strategy the β-reconstructed orientation map, reveal that a majority of β grains are oriented in the direction $<001>_\beta$ // Z. The Fig. 3 also highlights that the texture is more pronounced at the TOP regarding the IPF.

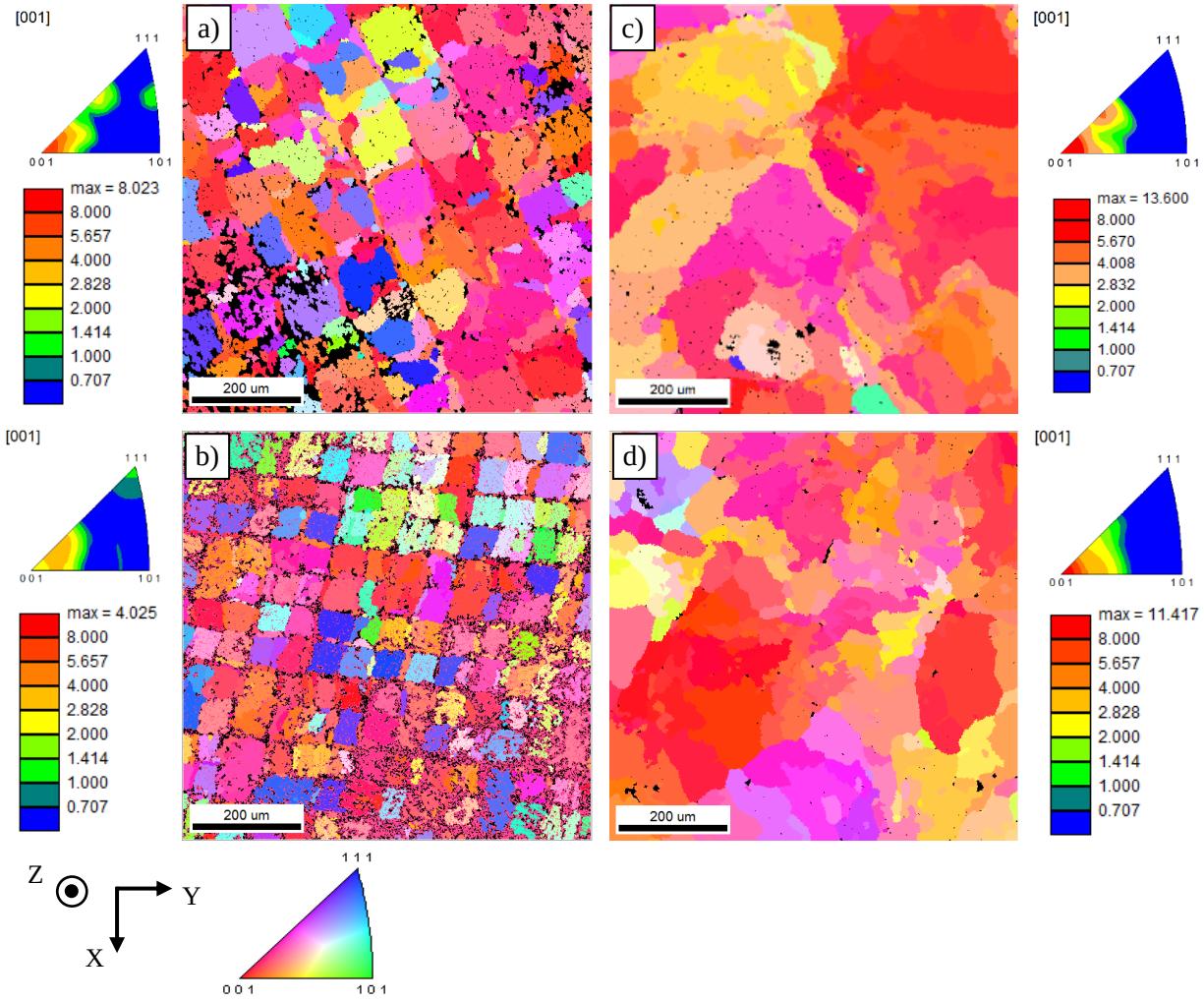

Fig. 3: EBSD [001] Inverse Pole Figure (IPF) orientation map of the reconstructed β phase with their corresponding [001] contour IPF. The β microstructure of CL strategy is observed on the (a) TOP and (b) BOTTOM of the bar and LB strategy is observed on the (c) TOP and (d) BOTTOM of a bar.

The β-phase proportion is correlated to the hardness; hardness globally decrease with the β-phase proportion [15]. To calculate the β proportion evolution along the building direction, a XRD measure is realized. The XRD spectra after pic separation are obtained from the TOP and the BOTTOM pellet with CL strategy are shown in Fig. 4 (a) and (b) respectively. The XRD spectra obtained from the TOP and the BOTTOM pellet with LB strategy are presented in Figs. 4 (c) and (d), respectively. The spectra are represented in χ range of 40-50°, because the $(110)_\beta$ and $(0002)_\alpha$ peaks are respectively reflected at 46.4° and 47.4°. For the pellets taken at the TOP of the bar, there is also a shift of XRD peaks towards higher angles. The calculated proportions of β phase in the samples are reported in Fig. 4 (e). At equilibrium state the β phase proportion is around 10% at room temperature for the Ti-6Al-4V alloy [16]. In this study the maximum β proportion is equal to 3.59% at the BOTTOM and 4.8 % at the TOP sample for CL strategy and about 3.34% at the BOTTOM and 2.6 % for the TOP with the LB strategy. The small proportion of β phase signals that the decomposition of α' into (α + β) is limited and not uniform.

Careful multiple micro indentation measurements on the (XY) planes on each pellets were conducted in order to measure the hardness. Fig. 4 (f) shows the average hardness values and reveals that hardness decreases with the number of layer deposit for the CL strategy with 395 HV on the BOTTOM and 365 HV on the TOP. For the LB strategy with 399 HV on the BOTTOM and 406 HV on the TOP the hardness is similar considering the incertitude. It should be noted that the hardness difference along the building direction is considering as significant only for CL strategy. The Fig. 4 (g) shows that the hardness globally decreases with the β-phase proportion. The LB strategy allows a better homogeneity of the hardness properties along the building direction

and this despite a greater β-phase proportion difference between the top and the bottom of the bar. It means that other parameters such as grain size or thermal history must play a role on hardness.

(e)

Sample	$CL_{(BOTTOM)}$	$CL_{(TOP)}$	$LB_{(BOTTOM)}$	$LB_{(TOP)}$
% β	3.59	4.80	4.34	2.61

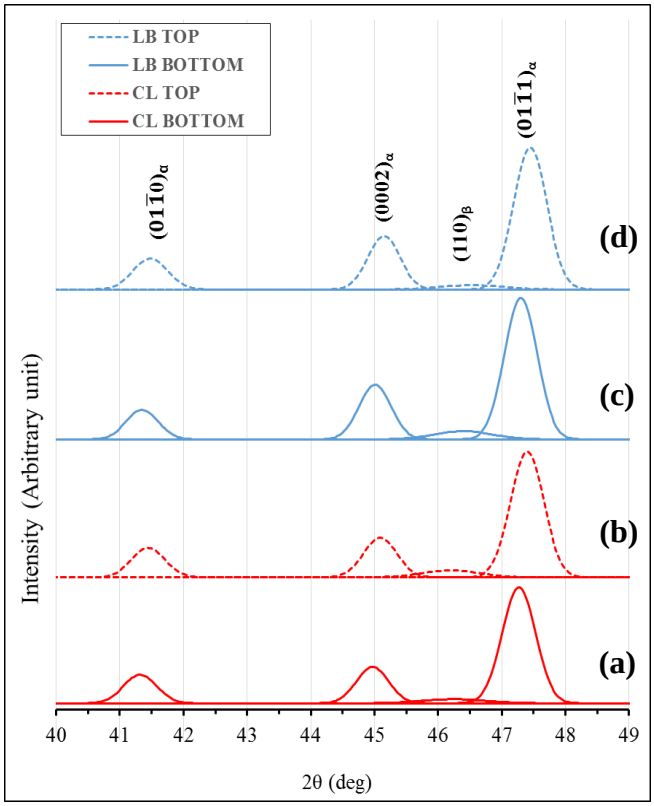

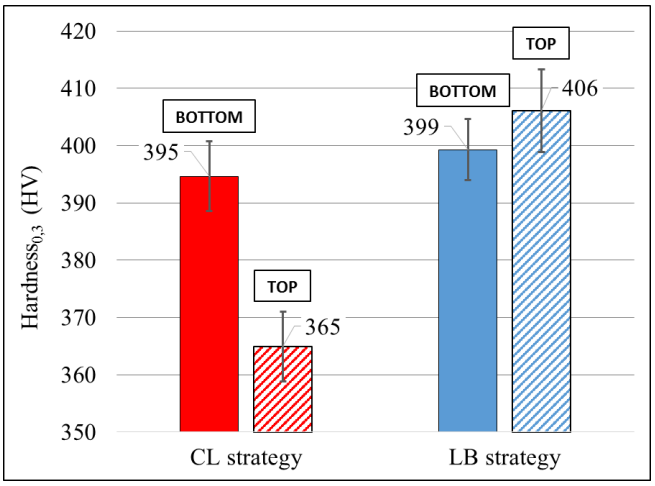

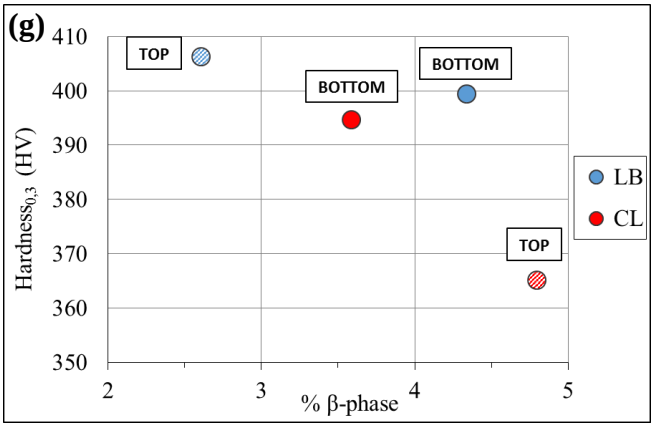

Fig. 4: XRD patterns of SLM-fabricated Ti–6Al–4V (XY) plane showing distinctive phase constituents: (a) CL strategy, BOTTOM pellet; (b) CL strategy, TOP pellet; (c) LB strategy, BOTTOM pellet; (d) LB strategy, TOP pellet. (e) Summary of β phase proportion measured by XRD of each sample. (f) Hardness measurements on (XY) plane of each sample. (e) Hardness evolution as a function of β -phase.

4. Discussion

The melt flow rate is 49 cm^3/h for the LB strategy and 13 cm^3/h for the CL strategy. Thus, the melt flow rate of LB strategy is more than three times higher than CL strategy with a larger melting area, therefore the LB strategy is interesting due to a faster melting process. The EBSD studies have shown that for both strategies, the resulting microstructure is composed of needles of α' martensitic that is consistent along the building direction. It is clear that the prior β-phase has a dominant <100>//Z solidification texture. However, the applied strategy changes the size and the organization of β grains. With the CL strategy, the β grain size (about 60µm) is related to the process parameters that lead to a paving structure and with the LB strategy, the β grains have an irregular shape and are bigger (110µm) due to the bigger melting area. For the CL strategy there is therefore a heterogeneity of microstructure along the manufacturing direction with β grains that grow up to 2 times the initial size as the number of layers increases. For the CL strategy, this evolution can be explained by grain growth selection. The LB strategy generates less microstructural and textural heterogeneities along the building direction. For the Ti-6Al-4V alloy, the β phase is more ductile than α' martensitic which means the increase of β-phase should imply a decrease of hardness of the sample [17]. Moreover the hardness usually increases with the decrease of grain size. In our study the grain size obtained with LB strategy is higher than the CL strategy however the hardness of the LB strategy is higher than the CL strategy. It is difficult to determine the cause of the change in hardness as it can be influenced by the grain size, the texture and the thermal history of the sample. However these results have shown that the hardness heterogeneity along the building direction is stronger with the CL strategy than

with the LB strategy. By using the LB strategy, the influence of Z-position on microstructural and mechanical properties is reduced and the texture is uniform along the Z-axis.

5. Conclusion

The influence of Z-position on microstructure and the mechanical properties of samples elaborated by the LB strategy and the CL strategy is compared. The following conclusions are drawn from this work:

- The melt flow rate of the LB strategy is three times higher than that of the CL strategy.
- The microstructure obtained by CL and LB strategies is a martensitic needle microstructure.
- Parent β grains are larger with the LB strategy and the CL strategy induces a paved grain structure. For both strategies, a heterogeneity of β microstructure is observed along the building direction thereby inducing β-grain magnification for the highest layers.
- The CL strategy induces a heterogeneity of hardness along the building direction that is influenced by the β proportion. The mechanical properties after application of the LB strategy are less influenced by the β proportion due to the strategy used.
- The LB strategy induces a better homogeneity of texture along the building direction than CL strategy.

To sum up, the LB strategy, performed with a larger Volume Energy Density, remains better in terms of texture and hardness homogeneity along the building direction. Moreover, it guaranties a higher melting rate.

References

[1] J. Kruth, L. Froyen, J. Vaerenbergh, P. Mercelis, M. Rombouts and B. Lauwers, "Selective laser melting of iron-based powder," *Journal of Materials Processing Technology,* vol. 149, pp. 616-622, 2004.

[2] S. Liu et Y. Shin, «Additive manufacturing of Ti-6Al-4V alloy : A review,» *Materials and Design,* vol. 164, 2019, 107552.

[3] D. Banerjee et J. Williams, «Perspectives on Titanium Science and Technology,» *Acta Materialia,* vol. 61, pp. 844-879, 2013.

[4] M. Simonelli, Y. Tse et C. Tuck, «On the Texture Formation of Selective Laser Melted Ti-6Al-4V,» *Metallurgical and Materials Transactions A,* vol. 45, pp. 2863-2872, 2014.

[5] L. Thijs, F. Verhaeghe, T. Craeghs, J. Van Humbeeck et J. Kruth, «A study of the microstructural evolution during selective laser melting of Ti-6Al-4V,» *Acta Materialia,* n° %158, pp. 3303-3312, 2010.

[6] P. Kumar, O. Prakash et U. Ramamurty, «Micro- and meso-structures and their influence on mechanical properties of SLM Ti-6Al-4V,» *Acta Materialia,* vol. 154, pp. 246-260, 2018.

[7] M. Neikter, A. Huang et X. Wu, «Microstructural characterization of binary microstructure pattern in selective laser-melted Ti-6Al-4V,» *The international Journal of Advanced Manufacturing Technology,* vol. 104, pp. 1381-1391, 2019.

[8] W. Xu, M. Brandt, S. Sun, J. Elambasseril, Q. Liu, K. Latham, K. Xia et M. Qian, «Additive manufacturing of strong and ductile Ti-6Al-4V by selective laser melting via in situ martensite decomposition,» *Acta Materialia,* vol. 85, pp. 74-84, 2015.

[9] M. Simonelli, Y. Tse and C. Tuck, "The formation of α + β microstructure in as-fabricated selective laser melting of Ti–6Al–4V," *Focus Issue: The Materials Science of Additive Manufacturing,* vol. 29, no. 17, pp. 2028-2035, 2014.

[10] J. Yang, H. Yu, J. Yin, M. Gao, Z. Wang et X. Zeng, «Formation and control of martensite in Ti-6Al-4V alloy produced by selective laser melting,» *Materials and Design,* vol. 108, pp. 308-318, 2016.

[11] T. DebRoy, H. Wei, J. Zuback, T. Muckherjee, J. Milewski, A. Beese, A. Wilson-Heid, A. De et W. Zhang, «Additive manufacturing,» *Progress in Materials Science,* vol. 92, pp. 112-224, 2018.

[12] M. Bach, N. Broll, A. Cornet et L. Gaide, «Diffraction X en traitement thermiques : dosage de l'austénite résiduelle par diffraction des rayons X,» *Journal de Physique IV,* vol. 6, pp. C4-887 - C4-895, 1996.

[13] M. Simonelli, Y. Tse et C. Tuck, «Further understanding of Ti-6Al-4V selective laser melting using texture analysis,» *23rd Annual International Solid Freeform Fabrication Symposium - An Additive Manufacturing Conference, SFF 2012,* pp. 480-491, 2012.

[14] C. Cayron, «ARPGE: a computer program to automatically reconstruct the parent grains from electron backscatter diffraction data,» *Journal of Applied Crystallography,* vol. 40, pp. 1183-1188, 2007.

[15] E. Magalini, L. Facchini, P. Robotti, A. Molinari, S. Höges et K. Wissenbach, «Ductility of a Ti-6Al-4V alloy produced by selective laser melting of prealloyed powders,» *Rapid prototyping journal,* vol. 16 (6), pp. 450-459, 2010.

[16] N. Gey, *THESE : Etude des changements de textures par transformation de phase β → α dans les produits TA6V laminés à chaud,* 1997.

[17] B. Vrancken, L. Thujs, J. Kruth et J. Humbeeck, «Heat treatment of Ti6Al4V produced by Selective Laser Melting: Microstructure and mechanical properties,» *Journal of Alloys and Compounds,* vol. 541, pp. 177-185, 2012.

[18] T. DebRoy, H. Wei, J. Zuback, T. Muckherjee, J. Elmer, J. Milewski, A. Beese, A. Wilson-Heid, A. De and W. Zhang, "Additive manufacturing," *Progress in Materials Science,* vol. 92, pp. 112-224, 2018.